HHS Public Access

Author manuscript

Neuroscience. Author manuscript; available in PMC 2020 September 01.

Published in final edited form as:

Neuroscience. 2019 September 01; 415: 77–88. doi:10.1016/j.neuroscience.2019.07.019.

Principal neurons in the anteroventral cochlear nucleus express cell-type specific glycine receptor α subunits

Shengyin Lin[1], **Ruili Xie**[1]

[1]Department of Otolaryngology, The Ohio State University, Columbus, OH

Abstract

Signal processing in the principal neurons of the anteroventral cochlear nucleus (AVCN) is modulated by glycinergic inhibition. The kinetics of IPSCs are specific to the target neurons. It remains unclear what glycine receptor subunits are involved in generating such target-specific IPSC kinetics in AVCN principal neurons. We investigated the expression patterns of glycine receptor α (GlyRα) subunits in AVCN using immunohistochemical labeling of four isoforms of GlyRα subunits (GlyRα$_1$ - α$_4$), and found that AVCN neurons express GlyRα$_1$ and GlyRα$_4$, but not GlyRα$_2$ and GlyRα$_3$ subunits. To further identify the cell type-specific expression patterns of GlyRα subunits, we combined whole-cell patch clamp recording with immunohistochemistry by recording from all three types of AVCN principal neurons, characterizing the synaptic properties of their glycinergic inhibition, dye-filling the neurons, and processing the slice for immunostaining of different GlyRα subunits. We found that AVCN bushy neurons express both GlyRα$_1$ and GlyRα$_4$ subunits that underlie their slow IPSC kinetics, whereas both T-stellate and D-stellate neurons express only GlyRα$_1$ subunit that underlies their fast IPSC kinetics. In conclusion, AVCN principal neurons express cell-type specific GlyRα subunits that underlie their distinct IPSC kinetics, which enables glycinergic inhibition from the same source to exert target cell-specific modulation of activity to support the unique physiological function of these neurons.

Keywords

Auditory; glycinergic inhibition; IPSC kinetics; bushy; T-stellate; D-stellate

INTRODUCTION

Acoustic information carried by the auditory nerve is first processed in the cochlear nucleus (CN), where different aspects of sound are segregated by various types of neurons and

Corresponding author: Ruili Xie, Ph.D, Department of Otolaryngology, The Ohio State University, 400 Tzagournis Medical Research Facility, 420 W 12th Ave, Columbus, OH 43210, Tel: 614-273-7271, ruili.xie@osumc.edu.

AUTHOR CONTRIBUTIONS

RX designed the work, RX and SL performed experiments and analyzed the data, RX wrote the manuscript.

DISCLOSURES

The authors have no competing financial interests to declare.

projected to different parallel pathways (Cant and Benson, 2003). In AVCN, the response properties of principal neurons are shaped by inhibition, which is predominantly glycinergic (Altschuler et al., 1986;Campagnola and Manis, 2014;Caspary et al., 1994;Gai and Carney, 2008;Keine et al., 2016;Kopp-Scheinpflug et al., 2002;Kuenzel et al., 2015;Nerlich et al., 2014;Wenthold et al., 1988). Our previous study (Xie and Manis, 2013) showed that glycinergic inhibition from the same source of dorsal cochlear nucleus (DCN) gives rise to drastically different IPSC kinetics in different AVCN principal neurons, and exerts cell type-specific modulatory effects that promote the temporal processing of sounds at different time scales. However, it remains unclear what mechanisms underlie such target-specific variations in IPSC kinetics.

Glycinergic inhibition with various IPSC kinetics have been widely observed throughout the nervous system (Balakrishnan et al., 2009;Legendre, 2001;Magnusson et al., 2005;Wassle et al., 2009). The main factor that determines IPSC kinetics lies in the subunit composition of glycine receptors (Lynch, 2009;Wassle, et al., 2009), among other mechanisms that relate to the process of transmitter release (Balakrishnan, et al., 2009;Magnusson, et al., 2005), receptor phosphorylation (Gentet and Clements, 2002) or intracellular chloride concentration (Pitt et al., 2008). Glycine receptors (GlyRs) are pentamers of α and β subunits in different stoichiometry (Burgos et al., 2016;Kuhse et al., 1993;Lynch, 2004), usually 2α3β or 3α2β (Durisic et al., 2012;Grudzinska et al., 2005). There are four isoforms of α subunits (α_1 - α_4) and only one β subunit. It is known that α subunits contain the ligand-binding sites and determine the kinetics of the inhibitory current, whereas the β subunit is auxiliary and facilitate receptor localization (Graham et al., 2006;Lynch, 2004;2009;Wassle, et al., 2009). Glycine receptors during embryonic development usually contain α_2 subunits, and gradually switch to α_1 subunits upon maturation (Lynch, 2009;Magnusson, et al., 2005;Takahashi et al., 1992). However, the scenario is not universally true in all brain regions. Indeed, all isoforms of α subunits were found in the adult nervous system with localized distributions (Blednov et al., 2015;Harvey et al., 2004;Lin et al., 2017;Lynch, 2009;Majumdar et al., 2009;Wassle, et al., 2009). In general, α_1 subunit-containing glycine receptors have faster IPSC kinetics than receptors with other α subunit isoforms (Gill et al., 2006;Harvey, et al., 2004;Majumdar, et al., 2009;Takahashi, et al., 1992;Veruki et al., 2007;Wassle, et al., 2009).

There are three major types of neurons in AVCN, including bushy, T-stellate (also named planar multipolar), and D-stellate (also named radiate multipolar) neurons, each of which exhibits unique features in morphology and intrinsic membrane properties, performs distinct transformation of auditory information, and projects to different target neurons (Cant and Benson, 2003;Doucet and Ryugo, 1997;Oertel, 1991;Oertel et al., 2011;Smith and Rhode, 1989). In particular, bushy neurons encode fine temporal information of sounds that are essential for auditory tasks such as sound localization that require high temporal precision (Joris and Yin, 2007). T-stellate neurons encode information with slower temporal features, such as sound envelope, which are important for auditory tasks like speech recognition (Blackburn and Sachs, 1990;May et al., 1998;Rhode and Greenberg, 1994;Shannon et al., 1995;Swaminathan and Heinz, 2012). Both bushy and T-stellate neurons are excitatory output neurons that project out of the AVCN to upper auditory nuclei (Cant and Benson, 2003). In contrast, D-stellate neurons are the main inhibitory interneurons of the CN that

respond to sounds over wide frequency ranges, and project locally within CN as well as to the contralateral CN (Arnott et al., 2004;Campagnola and Manis, 2014;Cant and Benson, 2003;Needham and Paolini, 2003;Nelken and Young, 1994) to improve temporal processing and promote signal detection in noise (Pressnitzer et al., 2001;Xie and Manis, 2013). Bushy neurons receive glycinergic inhibition with significantly slower IPSC kinetics than T-stellate neurons (Nerlich, et al., 2014;Xie and Manis, 2013;2014). Little is known about the synaptic properties of glycinergic inhibition in D-stellate neurons.

In this study, we examined the synaptic properties of glycinergic inhibition in all three types of AVCN principal neurons and determined the underlying glycine receptor α subunit composition. We found that bushy neurons showed slow IPSC kinetics with glycine receptors that contain both GlyRα$_1$ and GlyRα$_4$ subunits. In contrast, D-stellate neurons receive glycinergic inhibition from DCN with fast IPSC kinetics similar to those of T-stellate neurons, except that the synaptic strength is weaker with significantly smaller IPSC amplitude. Glycine receptors in both T- and D-stellate neurons contain GlyRα$_1$ subunits, but without any other α isoforms. We conclude that glycinergic inhibition, even from the same source, can exert target-specific modulatory effects through differences in glycine receptor α subunit compositions at the synapses on different neurons.

MATERIALS AND METHODS

CBA/CaJ mice of either sex at ages of postnatal day 29–89 were used for all the experiments except in one experiment of immunohistochemistry that used E14.5 mouse embryos. Mice were initially purchased from the Jackson Laboratory and maintained at the university animal facility. All experiments were performed under the guidelines of the protocols approved by the Institutional Animal Care and Use Committees at the University of Toledo and the Ohio State University.

Brain slice preparation

All electrophysiological recordings used parasagittal brain slices of cochlear nucleus prepared from CBA/CaJ mice (Xie, 2016;Xie and Manis, 2017). Briefly, mice were anesthetized with intraperitoneal injection of ketamine (100mg/kg) and xylazine (10mg/kg), decapitated, brainstem removed from the skull and transferred into artificial cerebral spinal fluid (ACSF), which was gassed with 5% CO_2 and 95% O_2 and pre-warmed to 34 °C. ACSF contained (in mM): 122 NaCl, 3 KCl, 1.25 NaH_2PO_4, 25 $NaHCO_3$, 20 glucose, 3 *myo-inositol,* 2 sodium pyruvate, 0.4 ascorbic acid, 2.5 $CaCl_2$ and 1.5 $MgSO_4$. Acute brain slices contained all three parts of the cochlear nucleus (AVCN, anteroventral cochlear nucleus; PVCN, posteroventral cochlear nucleus; and DCN, dorsal cochlear nucleus) were cut with a Vibratome 1000 (Technical Products, Inc.) at the thickness of either 400 μm (for cryostat re-sectioning and immunohistochemistry), 350 μm (for experiments with only electrophysiological recording), or 225 μm (for experiments with electrophysiological recording followed by immunohi stochemistry).

Cryostat re-sectioning and immunohistochemistry

In one set of the experiments, acute brain slices (400 μm in thickness) were immediately fixed with 4% paraformaldehyde in PBS after slicing, followed by PBS wash and overnight cryo-protection treatment in PBS with 30% sucrose. The cochlear nucleus slices were then embedded in Cryo-Gel (Cat#: 475237; Instrumedics Inc.) and re-sectioned in the same parasagittal orientation to 30 μm in thickness, using a cryostat slicer (Leica CM3050 S, Leica Biosystems). Re-sectioned slices were then double-stained with a primary antibody against vesicular glutamate transporter 1 (vGluT1) (polyclonal Guinea pig anti-vGluT1; Cat#: 135304, RRID: AB_887878; Synaptic Systems), and an antibody against one of the four glycine receptor α subunits, including glycine receptor α_1 subunit (polyclonal rabbit anti-GlyRα_1; Cat#: 146003, RRID: AB_2108989; Synapic Systems), α_2 subunit (polyclonal goat anti-GlyRα_2; Cat#: sc-17279, RRID: 2110230; Santa Cruz Biotechnology), α_3 subunit (polyclonal rabbit anti-GlyRα_3; Cat#: AGR-003, RRID: AB_2039889; Alomone Labs), and α_4 subunit (polyclonal rabbit anti-GlyRα_4; Cat#: AGR-015, RRID: AB_2340974; Alomone Labs). Two appropriate secondary antibodies were used in a combination of Goat anti-Guinea pig IgG conjugated with Alexa Fluor 488 (Cat#: A-11073, RRID: AB_142018; Molecular Probes), Rabbit anti-Goat IgG conjugated with Alexa Fluor 594 (Cat#: A-11080, RRID: AB_2534124; Thermo Fisher Scientific), or Goat anti-Rabbit IgG conjugated with Alexa Fluor 594 (Cat#: R37117, RRID: AB_2556545). Finally, DAPI Fluoromount-G mounting medium (Southern Biotech) was used to mount the slices and highlight the cell nucleus. Images were acquired using a confocal microscope (Leica TCS SP5, Leica Microsystems) at three different wavelengths for DAPI (to reveal cell nucleus), Alexa Fluor 488 (to reveal synaptic vesicles/terminals), and Alexa Fluor 594 (to reveal the staining of glycine receptor α subunits), respectively.

Whole-cell patch clamp recording

For electrophysiological recording, acute brain slices (350 or 225 μm in thickness) were incubated in gassed ACSF at 34 °C for ~45 minutes to allow recovery from the slicing, then transferred to a submersion chamber on a fixed-stage Axio Examiner microscope (Carl Zeiss Microscopy, LLC) and bathed in continuous flow of ACSF. Whole-cell patch clamp recording was performed using Multiclamp 700B amplifier, Axon Digidata 1550B digitizer, and pClamp 10 software (Molecular Devices). The recording pipette was pulled from KG-33 borosilicate glass (King Precision Glass) using a Sutter P-2000 puller (Sutter Instruments). Electrode solution contained (in mM): 105 K-gluconate, 36 KCl, 2 NaCl, 10 HEPES, 0.2 EGTA, 4 MgATP, 0.3 GTP, and 10 Tris-phosphocreatine, with pH adjusted to 7.2. All reported voltages were adjusted with a junction potential of −12 mV. To visualize cellular morphology, Alexa Fluor 488 (final concentration of 0.01% by weight) was added to the electrode solution for online fluorescent imaging as well as subsequent processing in immunohistochemistry. Five μM CNQX was added to the ACSF to block glutamatergic excitatory synaptic transmission. All recordings were made at 34 °C.

Under current clamp mode, membrane responses to depolarizing and hyperpolarizing step current injections were obtained from all three major cell types of the AVCN, including bushy, T-stellate and D-stellate neurons. Cell type was identified based on both electrophysiological and morphological features as described in previous studies (Brawer et

al., 1974;Cant and Morest, 1979;Wu and Oertel, 1984;Xie and Manis, 2013;2017). Specifically, bushy neurons were characterized by having short primary dendrites and heavily-branched tufts in resemble of a “bush” (Brawer, et al., 1974;Cant and Morest, 1979;Lauer et al., 2013;Webster and Trune, 1982), as well as firing only one or a few small spikes to prolonged suprathreshold current injections (Wu and Oertel, 1984). In contrast, both T- and D-stellate neurons had thin and long dendrites without heavily-branched tufts, and electrically fired tonic spikes to prolonged current injections (Fujino and Oertel, 2001;Wu and Oertel, 1984;Xie and Manis, 2017). T- and D-stellates were further distinguished by the orientation of their primary dendrites, in which T-stellate neurons have dendrites that ran parallel to the fascicles of auditory nerve fibers, while D-stellate neurons have dendrites spanned multiple fascicles (Doucet and Ryugo, 1997;Smith and Rhode, 1989;Xie and Manis, 2017). They also responded differently to large hyperpolarizing current injections, in which T-stellate neurons show slow and small depolarization sags, whereas D-stellate neurons show large and fast depolarization sags (Fujino and Oertel, 2001;Rodrigues and Oertel, 2006;Xie and Manis, 2017). Glycinergic IPSCs were obtained under voltage clamp mode in response to electrical stimulation at the DCN, which presumably activated the DCN tuberculoventral neurons that provide glycinergic inhibitory inputs to AVCN neurons (Muniak and Ryugo, 2014;Wickesberg and Oertel, 1990;Xie and Manis, 2013;2013;Zhang and Oertel, 1993). Stimulus pulse had a duration of 100 μs and was delivered via a 75 μm diameter concentric stimulating electrode (Frederick Haer Company). Stimulus amplitude was determined by gradually increasing the stimulus strength from zero until stimuli evoked reliable IPSCs in the target neuron.

Whole-cell recording followed by immunohistochemistry

After electrophysiological recording, the electrode pipette was slowly withdrawn until it detached from the patched neuron. In most cases, the patched neuron resealed and kept its morphology. Since the electrode solution contained Alexa Fluor 488, the resealed neuron was filled with the dye and thus labeled. The brain slices with thickness of 225 μm were then removed out of the recording chamber and fixed in PBS solution with 4% paraformaldehyde, followed by immunostaining procedure as described by Karadottir and Attwell (2006). Primary antibody against either $GlyR\alpha_1$ or $GlyR\alpha_4$ subunit was used, followed by corresponding secondary antibody as described above. Slices were cover-slipped and imaged for both the filled neuron (labeled with Alexa Fluor 488) and the staining of GlyRα subunits (labeled with Alexa Fluor 594) under a confocal microscope.

Data analysis

Electrophysiological data were analyzed using Igor Pro (Version 6.37, WaveMetrics). To quantify the intrinsic membrane properties of neurons, input resistance was calculated as the slope of the current-voltage relationship from hyperpolarizing responses to the four smallest levels of negative current injections. Membrane time constant was calculated as the average time constant from single exponential fits to the same four hyperpolarizing responses. Threshold current was defined as the minimum level of positive current pulse injection that triggered an action potential in the target neuron. Depolarization sag time constant was calculated as the time constant of the single exponential fit to the hyperpolarizing trace from the negative peak to the end of the current pulse (Xie and Manis, 2017). The relative

amplitude of the depolarization sag was calculated as the b/a ratio, whereas a and b are the amplitudes of the hyperpolarization peak and steady-state membrane voltage from the resting membrane potential, respectively (Fujino and Oertel, 2001;Xie and Manis, 2017). To quantify the kinetics of the glycinergic inhibition, IPSC decay time constant was obtained by fitting the IPSC decay phase with either a double exponential curve (best for bushy neurons) or a single exponential curve (best for T- and D-stellate neurons). The weighted decay time constant of an IPSC with double exponential curve fitting was calculated as: $\tau_w = \tau_{fast} \times A_{fast} + \tau_{slow} \times A_{slow}$, where A_{fast} and A_{slow} are the percent amplitude of the fast and slow component, and $A_{fast} + A_{fast} = 1$ (Xie and Manis, 2013).

Statistical analysis

All statistical analysis used GraphPad Prism (Version 6.0h, GraphPad Software). Population data were first analyzed with KS normality test to determine if they were normally distributed. Group comparisons were then performed with either one-way ANOVA (data with normal distribution) or Kruskal-Wallis test (data with non-normal distribution), followed by post-hoc multiple comparisons test if any significance was detected. Data are presented as mean ± standard deviation.

RESULTS

Electrophysiological properties of three types of principal neurons in AVCN

We performed whole-cell recording under current clamp mode from all three major cell types of AVCN: bushy (n = 21), T-stellate (n = 10) and D-stellate (n = 8) neurons. As shown in Figure 1A–C, positive current pulse injections evoked one or a few transient spikes in bushy neurons, but triggered tonic spikes throughout the duration of the current pulses in T- and D-stellate neurons. D-stellate neurons were further separated from T-stellate neurons in general by having fast depolarization sags in response to negative current injections (Fujino and Oertel, 2001;Rodrigues and Oertel, 2006;Xie and Manis, 2017). Cell classification was further confirmed with morphological features as previously reported (Xie and Manis, 2013;2017) (see Methods).

The electrophysiological properties of AVCN principal neurons showed significant differences among each other in most measurements except the resting membrane potential, as summarized in Table 1. In particular, bushy neurons showed significantly smaller input resistances than T-stellate (Dunn's multiple comparisons test: $p < 0.01$) and D-stellate (Dunn's multiple comparisons test: $p < 0.05$) neurons. The membrane time constant of T-stellate neurons was significantly higher than that of bushy (Tukey's multiple comparisons test: $p < 0.001$) and D-stellate (Tukey's multiple comparisons test: $p < 0.05$) neurons. Bushy neurons are less excitable and showed significantly higher threshold current than both T-stellate (Dunn's multiple comparisons test: $p < 0.001$) and D-stellate (Dunn's multiple comparisons test: $p < 0.05$) neurons. Hyperpolarization activated depolarization sags were fastest in D-stellate neurons with the smallest sag time constant among three cell types (Table 1). In particular, the difference between D-stellate and T-stellate neurons was significant (Dunn's multiple comparisons test: $p < 0.01$), which is a key differentiator as previously reported (Fujino and Oertel, 2001;Rodrigues and Oertel, 2006;Xie and Manis,

2017). D-stellate neurons also showed the smallest b/a ratio (Table 1), which is a measure influenced by faster kinetics of the hyperpolarization activated cation channels and/or larger I_h current amplitude. These differences in electrophysiological properties are consistent with various previous studies, and underlie the unique physiological function of each principal neuron in AVCN.

AVCN principal neurons show cell-type specific IPSC kinetics

To study glycinergic inhibition in AVCN principal neurons, IPSCs were recorded under voltage clamp mode at the holding potential of −112mV. Glycinergic inhibition was evoked by electrical stimulation of the DCN, which presumably activate the tuberculoventral neurons and antidromically the VCN D-stellate neurons. Consistent with our previous observations (Xie and Manis, 2013), IPSCs in bushy neurons were slower and the IPSC decay phase was best fit with a double exponential curve, while IPSCs in T-stellate neurons were fast and the decay was best fit with a single exponential curve (Figure 1D–E). Interestingly, the evoked IPSCs in D-stellate neurons showed fast kinetics like those in T-stellate neurons, and the IPSC decay was best fit with a single exponential curve (Figure 1F–G). As shown in Figure 1H, eIPSC decay time constants for both T- and D-stellate neurons were significantly smaller than that of bushy neurons (Tukey's multiple comparisons test: $p < 0.0001$), with no difference between each other (Tukey's multiple comparisons test: $p > 0.05$). However, the amplitude of evoked IPSC was significantly smaller in D-stellate neurons (Figure 1I and Table 1), suggesting that the glycinergic inhibition from DCN has weaker synaptic strength in D-stellate neurons.

AVCN neurons express glycine receptor α_1 and α_4 subunits

To study the underlying mechanisms of the different IPSC kinetics in AVCN principal neurons, we investigated the expression of kinetics-determining GlyRα subunits using immunohistochemistry. Parasagittal CN slices were re-sectioned to 30 μm thickness and stained using primary antibodies against vGluT1 (synaptic marker) and one of four GlyRα subunits (see Methods) (Figure 2). Cell nuclei were also labeled by DAPI included in the mounting medium. As shown in Figure 2A, all three parts of the CN were labeled well by GlyRα_1 antibody, along with vGluT1 and DAPI. Neurons in CN express α_1 subunit-containing glycine receptors, which is the adult form of GlyR in many brain regions. Further examination of the AVCN at high magnification showed that GlyRα_1 is expressed in different AVCN principal neurons. For example, vGluT1 labeled numerous ring-like structures that resemble the endbulb of Held terminals (Figure 2B, arrowheads), which surround AVCN bushy neurons. These same neurons were also labeled by GlyRα1 antibody, suggesting that GlyRs in AVCN bushy neurons contain GlyRα_1 subunits. In contrast, many other neurons that were prominently labeled by GlyRα_1 (Figure 2B, arrow), but only had small and few vGluT1 labeled puncta that were clearly not the endbulb of Held terminals. These neurons were likely stellate neurons (T- or D-stellate). Therefore, the data suggest that AVCN bushy and stellate neurons all express α_1 subunits in their GlyRs.

Staining with the antibody against GlyRα_4 subunit also labeled CN neurons (Figure 2G). Similar to GlyRα_1 staining in Figure 2B under high magnification, GlyRα_4 labeled puncta were clearly identifiable in putative bushy neurons with vGluT1 labeled endbulb of Held

terminals (Figure 2H, thick arrow), but not in putative stellate neurons (Figure 2H, thin arrow). In contrast, the same staining using primary antibodies against GlyRα$_2$ (Figure 2C) and GlyRα$_3$ subunits (Figure 2E) showed no detectable staining of either subunit. Examination of AVCN neurons at high magnification confirmed that no immunoreactivity was observed on either putative bushy (with vGluT1 labeled endbulb of Held terminal) or stellate neurons (Figure 2D and 2F). To test the efficiency of the antibodies, we performed additional immunostaining of GlyRα$_2$ in embryonic mouse brain at E14.5 (known to express GlyRα$_2$ subunit) (Lynch, 2009) and GlyRα$_3$ in mature mouse hippocampus (known to express GlyRα$_3$ subunit) (Eichler et al., 2009;Eichler et al., 2008). As expected, the GlyRα$_2$ antibody labeled embryonic neurons in the putative dorsal tier of thalamus (Figure 2Di). Similarly, the GlyRα$_3$ antibody labeled mature neurons in the hippocampus (Figure 2Fi).

All three types of principal neurons in AVCN express glycine receptor α$_1$ subunit

We performed a different set of experiments to definitively identify which AVCN principal neurons express what GlyRα subunits. We first performed whole-cell patch clamp recording in CN slices to characterize the cell types of target neurons, filled the neurons with fluorescent dye (Alexa Fluor 488), and then processed the slice for immunohistochemistry with primary antibody against either GlyRα$_1$ or GlyRα$_4$ subunit (see Methods). In these experiments, CN slices were cut at 225 μm thickness and remained throughout the process. Recorded neurons filled with Alexa Fluor 488 were tracked under a confocal microscope and imaged for the immunolabeling of GlyR α subunits.

As shown in Figure 3, all three major cell types of the AVCN were electrophysiologically and morphologically identified. The typical bushy neuron in Figure 3A fired only one action potential to positive current injection, and the neuron was surrounded by a ring of stained GlyRα$_1$ puncta (arrowheads, Figure 3B), along with many other labeled neurons (arrows). Similarly, GlyRα$_1$ puncta were observed in labeled T-stellate (Figure 3C–D) and D-stellate (Figure 3E–F) neurons. This set of experiments recorded 8 bushy neurons, 3 T-stellate and 3 D-stellate neurons, all were labeled by GlyRα$_1$ antibody. Consistent with the staining performed in cryostat-sectioned slices (Figure 2B), the results showed that all three types of principal neurons in AVCN express glycine receptors containing α$_1$ subunits.

Only bushy neurons express glycine receptor α$_4$ subunit

In a different set of experiments, we performed the same process as described above except the primary antibody against GlyRα$_4$ subunit was used instead. Despite of the weak staining and high level of non-specific background noise (see Discussion), labeling of GlyRα$_4$ was clearly recognizable. This set of experiments included 14 bushy neurons, 3 T-stellate and 4 D-stellate neurons. As shown in Figure 4, GlyRα$_4$ labeled puncta were seen on all filled bushy neurons, but not on any T-stellate or D-stellate neurons. Together with the observation in Figure 2H, we conclude that GlyRα$_4$ subunit is expressed only by bushy neurons and not by T- or D-stellate neurons.

In summary, AVCN bushy neurons receive glycinergic inhibition with slow IPSC kinetics, and express glycine receptors that contain both GlyRα$_1$ and α$_4$ subunits. In contrast, both T-

stellate and D-stellate neurons receive glycinergic inhibition with fast IPSC kinetics, and express glycine receptors with only GlyRα$_1$ subunits.

DISCUSSION

Inhibition is an essential component of the nervous system and helps to shape the normal function of neurons. Given the diversity in neuronal cell types and their physiological function in the brain, it is imperative to understand how different inhibitory effects are achieved in different neurons, especially within local neural circuits where the same shared inhibitory input differentially modulate distinct target neurons. We investigated the mechanisms of inhibition in the AVCN, where the local auditory neural network consists of three types of principal neurons with well-characterized anatomy and physiology. Our previous study showed that the input from the DCN produces glycinergic inhibition with target cell-specific IPSC kinetics in AVCN bushy and T-stellate neurons, and differentially modulates their temporal processing at different time scales (Xie and Manis, 2013). In this study, we combined electrophysiology with immunohistochemistry to demonstrate that the underlying mechanism of different IPSC kinetics in different AVCN principal neurons is due to target cell-specific GlyRα subunit composition. The study further shows that D-stellate neurons are also modulated by glycinergic inhibition, and have fast IPSC kinetics like those seen in T-stellate neurons but with significantly weaker synaptic strength. Our findings provide an example of how different glycine receptor α subunit isoforms are employed in a local neural circuit with a shared inhibitory input, to differentially modulate the distinct physiological function of various target neurons.

Staining quality in thick slices after patch clamp recordings

We combined patch clamp recording with immunohistochemistry to both obtain the physiological data and identify the expression patterns of GlyRα subunits from the same individual neurons (Figures 3 and 4). While this is a very powerful technique, the quality of the staining was not as robust as those that used cryostat-sectioned slices. For example, in the staining of the GlyRα$_1$ subunit, slices with recorded neurons showed relatively higher background noise (Figure 3B, D, F) compared with cryostat-sectioned slices (Figure 2B). Whereas in the staining of the GlyRα$_4$ subunit, some staining showed noticeable labeling of large unknown patches (Figure 4B) that resemble either small cells or cell nuclei, which were not seen in cryostat-sectioned slices (Figure 2H). It was likely caused by the long recording procedure (usually 2–3 hours including the recovery incubation prior to the recording) before the slices were fixed for immunohistochemistry (Figures 3, 4). In comparison, acute brain slices were cut and immediately fixed for re-slicing in cryostat-sectioned slices (Figure 2), which would better preserve cellular structure with less debris and thus reduced non-specific labeling. In addition, tissue thickness might also play some role in the staining quality, as recorded slices were at 225 μm and cryostat-sectioned slices were at 30 pm. Ways that might further optimize the staining process were discussed in details by Karadottir and Attwell (2006). In this study, despite the higher background noise associated with this technique, our experiments showed clearly identifiable labeling of GlyRα subunits, which were consistent with the results from our experiments using cryostat-sectioned slices.

Glycinergic inhibition in bushy neurons with slow IPSC kinetics

A previous report in rats showed that bushy neurons express GlyRα$_1$ subunits (Hruskova et al., 2012). However, it is unlikely that α$_1$ is the only isoform expressed in bushy neurons, since the adult form receptor with α$_1$β composition is known to have the fastest IPSC kinetics among all glycine receptors (Gill, et al., 2006;Harvey, et al., 2004;Majumdar, et al., 2009;Takahashi, et al., 1992;Veruki, et al., 2007;Wassle, et al., 2009). The significantly slower IPSC kinetics exhibited in bushy neurons suggests that these neurons express multiple isoforms of GlyRα subunit. We previously speculated that bushy neurons may express GlyRα$_2$ subunit (Xie and Manis, 2013), which would align with the report that low levels of GlyRα$_2$ mRNAs persist in the rat auditory brainstem during early postnatal development (up to P20) (Piechotta et al., 2001). However, we did not detect GlyRα$_2$ in this study, suggesting that GlyRα$_2$ may have already phased out at the age range of the mice we used (P29–89). Instead, we found that bushy neurons express α$_4$ subunits in addition to α$_1$, with possible stoichiometry of glycine receptors that include α$_1$α$_4$3β, 2α$_1$α$_4$2β, and α$_1$2α$_4$2β (Durisic, et al., 2012;Grudzinska, et al., 2005). It remains unclear when and how different α subunit isoforms transition through developmental stages in bushy neurons.

Glycinergic inhibition with slow IPSC kinetics was shown to paradoxically fine-tune the spike timing of auditory signals in bushy neurons at the time scale of tens of microseconds (Xie and Manis, 2013). It does so through a slow tonic inhibitory effect that functions as a high-pass filter to prevent smaller auditory nerve inputs with slower and untimely EPSPs from triggering action potentials in bushy neurons, thus reducing firing probability but improving temporal precision of the output signals to the superior olivary complex (Kuenzel et al., 2011;Nerlich, et al., 2014;Xie and Manis, 2013). The IPSC kinetics can be further modulated dynamically based on the activity levels of the auditory nerve input (Kuenzel, et al., 2015;Nerlich et al., 2014;Nerlich, et al., 2014).

Glycinergic inhibition in T-stellate neurons

The finding that T-stellate neurons only express GlyRα$_1$ subunits is not surprising, given that the kinetics of the IPSCs in T-stellate neurons (~ 1.3 ms) is among the fastest in the entire nervous system (Gill, et al., 2006;Harvey, et al., 2004;Lu et al., 2008;Lynch, 2009;Magnusson, et al., 2005;Wassle, et al., 2009;Xie and Manis, 2013). The glycine receptors in T-stellate neurons are likely α$_1$β heteromers with stoichiometry of 2α$_1$3β or 3α$_1$2β.

Unlike bushy neurons, T-stellate neurons have significantly slower membrane time constants and higher input resistances, which enable greater impact of phasic inhibition with fast IPSCs to both effectively and promptly hyperpolarize the membrane potential to eliminate poorly timed spikes in T-stellate neurons (Xie and Manis, 2013). Glycinergic inhibition improves the spike timing of T-stellate neurons on a timescale of milliseconds, which is slower than its effect in bushy neurons, but ideal for their physiological function of encoding slower sound envelopes (Gai and Carney, 2008;Rhode and Greenberg, 1994;Wang and Sachs, 1994;Xie and Manis, 2013). Tests in computer models showed that fast IPSC kinetics are essential to the optimal function of the glycinergic inhibition in T-stellate neurons, and the same is true for slower IPSC kinetics in bushy neurons (Xie and Manis, 2013).

Glycinergic inhibition in D-stellate neurons

D-stellate neurons are inhibitory neurons in the VCN that provide wide-band glycinergic inhibition to various cell types throughout the cochlear nucleus (Arnott, et al., 2004;Needham and Paolini, 2003;Palmer et al., 2003;Paolini and Clark, 1999;Smith and Rhode, 1989). It has been shown that D-stellate neurons themselves receive inhibitory inputs from unidentified sources (Ferragamo et al., 1998;Paolini and Clark, 1999;Smith and Rhode, 1989), including possibly the DCN tuberculoventral neurons (Saint Marie et al., 1991;Wickesberg and Oertel, 1990;Zhang and Oertel, 1993) as well as other D-stellate neurons of the VCN (Arnott, et al., 2004;Ferragamo, et al., 1998;Smith and Rhode, 1989). In this study, stimulating the DCN could activate both inhibitory sources of the CN, including the DCN tuberculoventral neurons as well as the VCN D-stellate neurons, which are known to project to DCN and therefore can be antidromically activated in this stimulating paradigm. The fast kinetics of evoked IPSCs (Figure 1F) implies little or no dendritic filtering of the recorded current, which indicates that the inhibitory synapses are physically close to the recording sites and localize near the somata or proximal dendrites, consistent with previous studies using electron microscope (Smith and Rhode, 1989).

The finding that both D-stellate and T-stellate neurons have fast IPSCs with no significant difference in their decay time constants (Figure 1G–H) agrees with the immunostaining results that both express only GlyRα_1 subunit (Figures 3 – 4). Given the similarity in their intrinsic membrane properties (Figure 1B–C), fast inhibition may work in the same way in shaping the responses of D-stellate neurons as it does in T-stellate neurons (Xie and Manis, 2013), i.e. through timely hyperpolarization to terminate prolonged excitation in D-stellate neurons and promptly stop the inhibitory innervation onto their target neurons. It is unclear if such fast inhibition would contribute to the creation of onset firing pattern of D-stellate neurons (Smith and Rhode, 1989;Winter and Palmer, 1995). Interestingly, the amplitude of evoked IPSCs in D-stellate neurons was significantly smaller than that of T-stellate neurons, suggesting that the inhibition have weaker synaptic strength in D-stellate neurons.

Distinct combination of EPSC and IPSC kinetics in AVCN principal neurons

In addition to the cell type-specific IPSC kinetics of their inhibitory inputs, AVCN principal neurons are also innervated by excitatory inputs from the auditory nerve with cell type-specific EPSC kinetics (Cao and Oertel, 2010;Gardner et al., 1999;2001;Xie and Manis, 2013;2017). Remarkably, the kinetics of EPSCs and IPSCs are intermingled in different AVCN principle neurons. Bushy neurons, which receive inhibition with slow IPSC kinetics with an average decay time constant of 8–11ms (Figure 1; Xie and Manis, 2013), are innervated by excitatory inputs that have extremely fast EPSC kinetics with an average decay time constant of ~ 0.35 ms (Gardner, et al., 2001;Manis et al., 2011;Xie and Manis, 2013). T-stellate neurons show fast kinetics in both IPSCs (decay time constant of 1.1 −1.3 ms) (Figure 1; Xie and Manis, 2013) and EPSCs (decay time constant of 0.41–0.62 ms) (Gardner, et al., 2001;Manis, et al., 2011;Xie and Manis, 2013;2017). In contrast, D-stellate neurons receive fast IPSCs (decay time constant of 1.6 ms) (Figure 1) but drastically slower EPSCs (decay time constant of ~5 ms) (Xie and Manis, 2017). The distinct properties of EPSC and IPSC kinetics in each AVCN principal neurons are generated by the different combinations of glutamate and glycine receptors they express, as well as other factors that

may include synaptic location, number of converged synaptic inputs, cellular morphology, and composition of various ion channels (Gardner, et al., 2001;Manis, et al., 2011;White et al., 1994;Xie and Manis, 2017), all of which help define the unique response properties of each AVCN neuron and contribute to its distinct physiological function in processing sound information from the environment.

ACKNOWLEDGEMENTS

We thank Y. Wang and B. J. Seicol for their comments on the manuscript

FUNDING

This work was supported by US National Institute on Deafness and other Communication Disorders grants R03DC013396 and R01DC016037 to RX.

REFERENCES

Altschuler RA, Betz H, Parakkal MH, Reeks KA, Wenthold RJ (1986), Identification of glycinergic synapses in the cochlear nucleus through immunocytochemical localization of the postsynaptic receptor. Brain Res 369:316–320. [PubMed: 3008938]

Arnott RH, Wallace MN, Shackleton TM, Palmer AR (2004), Onset neurones in the anteroventral cochlear nucleus project to the dorsal cochlear nucleus. J Assoc Res Otolaryngol 5:153–170. [PubMed: 15357418]

Balakrishnan V, Kuo SP, Roberts PD, Trussell LO (2009), Slow glycinergic transmission mediated by transmitter pooling. Nat Neurosci 12:286–294. [PubMed: 19198604]

Blackburn CC, Sachs MB (1990), The representations of the steady-state vowel sound /e/ in the discharge patterns of cat anteroventral cochlear nucleus neurons. J Neurophysiol 63:1191–1212. [PubMed: 2358869]

Blednov YA, Benavidez JM, Black M, Leiter CR, Osterndorff-Kahanek E, Harris RA (2015), Glycine receptors containing alpha2 or alpha3 subunits regulate specific ethanol-mediated behaviors. The Journal of pharmacology and experimental therapeutics 353:181–191. [PubMed: 25678534]

Brawer JR, Morest DK, Kane EC (1974), The neuronal architecture of the cochlear nucleus of the cat. J Comp Neurol 155:251–300. [PubMed: 4134212]

Burgos CF, Yevenes GE, Aguayo LG (2016), Structure and Pharmacologic Modulation of Inhibitory Glycine Receptors. Mol Pharmacol 90:318–325. [PubMed: 27401877]

Campagnola L, Manis PB (2014), A map of functional synaptic connectivity in the mouse anteroventral cochlear nucleus. J Neurosci 34:2214–2230. [PubMed: 24501361]

Cant NB, Benson CG (2003), Parallel auditory pathways: projection patterns of the different neuronal populations in the dorsal and ventral cochlear nuclei. Brain research bulletin 60:457–474. [PubMed: 12787867]

Cant NB, Morest DK (1979), Organization of the neurons in the anterior division of the anteroventral cochlear nucleus of the cat. Light-microscopic observations. Neuroscience 4:1909–1923. [PubMed: 530438]

Cao XJ, Oertel D (2010), Auditory nerve fibers excite targets through synapses that vary in convergence, strength, and short-term plasticity. J Neurophysiol 104:2308–2320. [PubMed: 20739600]

Caspary DM, Backoff PM, Finlayson PG, Palombi PS (1994), Inhibitory inputs modulate discharge rate within frequency receptive fields of anteroventral cochlear nucleus neurons. J Neurophysiol 72:2124–2133. [PubMed: 7884448]

Doucet JR, Ryugo DK (1997), Projections from the ventral cochlear nucleus to the dorsal cochlear nucleus in rats. J Comp Neurol 385:245–264. [PubMed: 9268126]

Durisic N, Godin AG, Wever CM, Heyes CD, Lakadamyali M, Dent JA (2012), Stoichiometry of the human glycine receptor revealed by direct subunit counting. J Neurosci 32:12915–12920. [PubMed: 22973015]

Eichler SA, Forstera B, Smolinsky B, Juttner R, Lehmann TN, Fahling M, Schwarz G, Legendre P, et al. (2009), Splice-specific roles of glycine receptor alpha3 in the hippocampus. The European journal of neuroscience 30:1077–1091. [PubMed: 19723286]

Eichler SA, Kirischuk S, Juttner R, Schaefermeier PK, Legendre P, Lehmann TN, Gloveli T, Grantyn R, et al. (2008), Glycinergic tonic inhibition of hippocampal neurons with depolarizing GABAergic transmission elicits histopathological signs of temporal lobe epilepsy. J Cell Mol Med 12:2848–2866. [PubMed: 19210758]

Ferragamo MJ, Golding NL, Oertel D (1998), Synaptic inputs to stellate cells in the ventral cochlear nucleus. J Neurophysiol 79:51–63. [PubMed: 9425176]

Fujino K, Oertel D (2001), Cholinergic modulation of stellate cells in the mammalian ventral cochlear nucleus. J Neurosci 21:7372–7383. [PubMed: 11549747]

Gai Y, Carney LH (2008), Influence of inhibitory inputs on rate and timing of responses in the anteroventral cochlear nucleus. J Neurophysiol 99:1077–1095. [PubMed: 18199821]

Gardner SM, Trussell LO, Oertel D (1999), Time course and permeation of synaptic AMPA receptors in cochlear nuclear neurons correlate with input. J Neurosci 19:8721–8729. [PubMed: 10516291]

Gardner SM, Trussell LO, Oertel D (2001), Correlation of AMPA receptor subunit composition with synaptic input in the mammalian cochlear nuclei. J Neurosci 21:7428–7437. [PubMed: 11549753]

Gentet LJ, Clements JD (2002), Binding site stoichiometry and the effects of phosphorylation on human alpha1 homomeric glycine receptors. J Physiol 544:97–106. [PubMed: 12356883]

Gill SB, Veruki ML, Hartveit E (2006), Functional properties of spontaneous IPSCs and glycine receptors in rod amacrine (AII) cells in the rat retina. J Physiol 575:739–759. [PubMed: 16825305]

Graham BA, Schofield PR, Sah P, Margrie TW, Callister RJ (2006), Distinct physiological mechanisms underlie altered glycinergic synaptic transmission in the murine mutants spastic, spasmodic, and oscillator. J Neurosci 26:4880–4890. [PubMed: 16672662]

Grudzinska J, Schemm R, Haeger S, Nicke A, Schmalzing G, Betz H, Laube B (2005), The beta subunit determines the ligand binding properties of synaptic glycine receptors. Neuron 45:727–739. [PubMed: 15748848]

Harvey RJ, Depner UB, Wassle H, Ahmadi S, Heindl C, Reinold H, Smart TG, Harvey K, et al. (2004), GlyR alpha3: an essential target for spinal PGE2-mediated inflammatory pain sensitization. Science 304:884–887. [PubMed: 15131310]

Hruskova B, Trojanova J, Kulik A, Kralikova M, Pysanenko K, Bures Z, Syka J, Trussell LO, et al. (2012), Differential distribution of glycine receptor subtypes at the rat calyx of Held synapse. J Neurosci 32:17012–17024. [PubMed: 23175852]

Joris P, Yin TC (2007), A matter of time: internal delays in binaural processing. Trends Neurosci 30:70–78. [PubMed: 17188761]

Karadottir R, Attwell D (2006), Combining patch-clamping of cells in brain slices with immunocytochemical labeling to define cell type and developmental stage. Nat Protoc 1:1977–1986. [PubMed: 17487186]

Keine C, Rubsamen R, Englitz B (2016), Inhibition in the auditory brainstem enhances signal representation and regulates gain in complex acoustic environments. eLife 5.

Kopp-Scheinpflug C, Dehmel S, Dorrscheidt GJ, Rubsamen R (2002), Interaction of excitation and inhibition in anteroventral cochlear nucleus neurons that receive large endbulb synaptic endings. J Neurosci 22:11004–11018. [PubMed: 12486196]

Kuenzel T, Borst JG, van der Heijden M (2011), Factors controlling the input-output relationship of spherical bushy cells in the gerbil cochlear nucleus. J Neurosci 31:4260–4273. [PubMed: 21411667]

Kuenzel T, Nerlich J, Wagner H, Rubsamen R, Milenkovic I (2015), Inhibitory properties underlying non-monotonic input-output relationship in low-frequency spherical bushy neurons of the gerbil. Frontiers in neural circuits 9:14. [PubMed: 25873864]

Kuhse J, Laube B, Magalei D, Betz H (1993), Assembly of the inhibitory glycine receptor: identification of amino acid sequence motifs governing subunit stoichiometry. Neuron 11:1049–1056. [PubMed: 8274276]

Lauer AM, Connelly CJ, Graham H, Ryugo DK (2013), Morphological Characterization of Bushy Cells and Their Inputs in the Laboratory Mouse (Mus musculus) Anteroventral Cochlear Nucleus. PLoS One 8:e73308. [PubMed: 23991186]

Legendre P (2001), The glycinergic inhibitory synapse. Cell Mol Life Sci 58:760–793. [PubMed: 11437237]

Lin MS, Xiong WC, Li SJ, Gong Z, Cao X, Kuang XJ, Zhang Y, Gao TM, et al. (2017), alpha2-glycine receptors modulate adult hippocampal neurogenesis and spatial memory. Dev Neurobiol 77:1430–1441. [PubMed: 29057625]

Lu T, Rubio ME, Trussell LO (2008), Glycinergic transmission shaped by the corelease of GABA in a mammalian auditory synapse. Neuron 57:524–535. [PubMed: 18304482]

Lynch JW (2004), Molecular structure and function of the glycine receptor chloride channel. Physiol Rev 84:1051–1095. [PubMed: 15383648]

Lynch JW (2009), Native glycine receptor subtypes and their physiological roles. Neuropharmacology 56:303–309. [PubMed: 18721822]

Magnusson AK, Kapfer C, Grothe B, Koch U (2005), Maturation of glycinergic inhibition in the gerbil medial superior olive after hearing onset. J Physiol 568:497–512. [PubMed: 16096336]

Majumdar S, Weiss J, Wassle H (2009), Glycinergic input of widefield, displaced amacrine cells of the mouse retina. J Physiol 587:3831–3849. [PubMed: 19528249]

Manis PB, Xie R, Wang Y, Marrs GS, Spirou GA (2011) The Endbulbs of Held In: Synaptic Mechanisms in the Auditory System, vol. (Trussell LO, Popper AN, Fay RR, eds), pp. 61–93. New York: Springer.

May BJ, Prell GS, Sachs MB (1998), Vowel representations in the ventral cochlear nucleus of the cat: effects of level, background noise, and behavioral state. J Neurophysiol 79:1755–1767. [PubMed: 9535945]

Muniak MA, Ryugo DK (2014), Tonotopic organization of vertical cells in the dorsal cochlear nucleus of the CBA/J mouse. J Comp Neurol 522:937–949. [PubMed: 23982998]

Needham K, Paolini AG (2003), Fast inhibition underlies the transmission of auditory information between cochlear nuclei. J Neurosci 23:6357–6361. [PubMed: 12867521]

Nelken I, Young ED (1994), Two separate inhibitory mechanisms shape the responses of dorsal cochlear nucleus type IV units to narrowband and wideband stimuli. J Neurophysiol 71:2446–2462. [PubMed: 7931527]

Nerlich J, Keine C, Rubsamen R, Burger RM, Milenkovic I (2014), Activity-dependent modulation of inhibitory synaptic kinetics in the cochlear nucleus. Frontiers in neural circuits 8:145. [PubMed: 25565972]

Nerlich J, Kuenzel T, Keine C, Korenic A, Rubsamen R, Milenkovic I (2014), Dynamic fidelity control to the central auditory system: synergistic glycine/GABAergic inhibition in the cochlear nucleus. J Neurosci 34:11604–11620. [PubMed: 25164657]

Oertel D (1991), The role of intrinsic neuronal properties in the encoding of auditory information in the cochlear nuclei. Curr Opin Neurobiol 1:221–228. [PubMed: 1821185]

Oertel D, Wright S, Cao XJ, Ferragamo M, Bal R (2011), The multiple functions of T stellate/multipolar/chopper cells in the ventral cochlear nucleus. Hear Res 276:61–69. [PubMed: 21056098]

Palmer AR, Wallace MN, Arnott RH, Shackleton TM (2003), Morphology of physiologically characterised ventral cochlear nucleus stellate cells. Exp Brain Res 153:418–426. [PubMed: 12955380]

Paolini AG, Clark GM (1999), Intracellular responses of onset chopper neurons in the ventral cochlear nucleus to tones: evidence for dual-component processing. J Neurophysiol 81:2347–2359. [PubMed: 10322071]

Piechotta K, Weth F, Harvey RJ, Friauf E (2001), Localization of rat glycine receptor alpha1 and alpha2 subunit transcripts in the developing auditory brainstem. J Comp Neurol 438:336–352. [PubMed: 11550176]

Pitt SJ, Sivilotti LG, Beato M (2008), High intracellular chloride slows the decay of glycinergic currents. J Neurosci 28:11454–11467. [PubMed: 18987182]

Pressnitzer D, Meddis R, Delahaye R, Winter IM (2001), Physiological correlates of comodulation masking release in the mammalian ventral cochlear nucleus. J Neurosci 21:6377–6386. [PubMed: 11487661]

Rhode WS, Greenberg S (1994), Encoding of amplitude modulation in the cochlear nucleus of the cat. J Neurophysiol 71:1797–1825. [PubMed: 8064349]

Rodrigues AR, Oertel D (2006), Hyperpolarization-activated currents regulate excitability in stellate cells of the mammalian ventral cochlear nucleus. J Neurophysiol 95:76–87. [PubMed: 16192334]

Saint Marie RL, Benson CG, Ostapoff EM, Morest DK (1991), Glycine immunoreactive projections from the dorsal to the anteroventral cochlear nucleus. Hear Res 51:11–28. [PubMed: 1672865]

Shannon RV, Zeng FG, Kamath V, Wygonski J, Ekelid M (1995), Speech recognition with primarily temporal cues. Science 270:303–304. [PubMed: 7569981]

Smith PH, Rhode WS (1989), Structural and functional properties distinguish two types of multipolar cells in the ventral cochlear nucleus. J Comp Neurol 282:595–616. [PubMed: 2723154]

Swaminathan J, Heinz MG (2012), Psychophysiological analyses demonstrate the importance of neural envelope coding for speech perception in noise. J Neurosci 32:1747–1756. [PubMed: 22302814]

Takahashi T, Momiyama A, Hirai K, Hishinuma F, Akagi H (1992), Functional correlation of fetal and adult forms of glycine receptors with developmental changes in inhibitory synaptic receptor channels. Neuron 9:1155–1161. [PubMed: 1281418]

Veruki ML, Gill SB, Hartveit E (2007), Spontaneous IPSCs and glycine receptors with slow kinetics in wide-field amacrine cells in the mature rat retina. J Physiol 581:203–219. [PubMed: 17331993]

Wang X, Sachs MB (1994), Neural encoding of single-formant stimuli in the cat. II. Responses of anteroventral cochlear nucleus units. J Neurophysiol 71:59–78. [PubMed: 8158242]

Wassle H, Heinze L, Ivanova E, Majumdar S, Weiss J, Harvey RJ, Haverkamp S (2009), Glycinergic transmission in the Mammalian retina. Front Mol Neurosci 2:6. [PubMed: 19924257]

Webster DB, Trune DR (1982), Cochlear nuclear complex of mice. Am J Anat 163:103–130. [PubMed: 7072613]

Wenthold RJ, Parakkal MH, Oberdorfer MD, Altschuler RA (1988), Glycine receptor immunoreactivity in the ventral cochlear nucleus of the guinea pig. J Comp Neurol 276:423–435. [PubMed: 2848063]

White JA, Young ED, Manis PB (1994), The electrotonic structure of regular-spiking neurons in the ventral cochlear nucleus may determine their response properties. J Neurophysiol 71:1774–1786. [PubMed: 8064348]

Wickesberg RE, Oertel D (1990), Delayed, frequency-specific inhibition in the cochlear nuclei of mice: a mechanism for monaural echo suppression. J Neurosci 10:1762–1768. [PubMed: 1972392]

Winter IM, Palmer AR (1995), Level dependence of cochlear nucleus onset unit responses and facilitation by second tones or broadband noise. J Neurophysiol 73:141–159. [PubMed: 7714560]

Wu SH, Oertel D (1984), Intracellular injection with horseradish peroxidase of physiologically characterized stellate and bushy cells in slices of mouse anteroventral cochlear nucleus. J Neurosci 4:1577–1588. [PubMed: 6726347]

Xie R (2016), Transmission of auditory sensory information decreases in rate and temporal precision at the endbulb of Held synapse during age-related hearing loss. J Neurophysiol 116:2695–2705. [PubMed: 27683884]

Xie R, Manis PB (2013), Glycinergic synaptic transmission in the cochlear nucleus of mice with normal hearing and age-related hearing loss. J Neurophysiol: doi: 10.1152/jn.00151.02013.

Xie R, Manis PB (2013), Target-specific IPSC kinetics promote temporal processing in auditory parallel pathways. J Neurosci 33:1598–1614. [PubMed: 23345233]

Xie R, Manis PB (2014), GABAergic and glycinergic inhibitory synaptic transmission in the ventral cochlear nucleus studied in VGAT channelrhodopsin-2 mice. Frontiers in neural circuits 8:84. [PubMed: 25104925]

Xie R, Manis PB (2017), Radiate and planar multipolar neurons of the mouse anteroventral cochlear nucleus: Intrinsic excitability and characterization of their auditory nerve input. Frontiers in neural circuits.

Xie R, Manis PB (2017), Synaptic transmission at the endbulb of Held deteriorates during age-related hearing loss. J Physiol 595:919–934. [PubMed: 27618790]

Zhang S, Oertel D (1993), Tuberculoventral cells of the dorsal cochlear nucleus of mice: intracellular recordings in slices. J Neurophysiol 69:1409–1421. [PubMed: 8389823]

HIGHLIGHT

- Glycine receptor α subunit composition underlies cell type-specific IPSC kinetics in AVCN
- AVCN expresses glycine receptor α_1 and α_4, but not α_2 and α_3 subunits
- Bushy neurons express both α_1 and α_4 that underlie slow IPSC kinetics
- T-stellate and D-stellate neurons express only α_1 that underlies fast IPSC kinetics

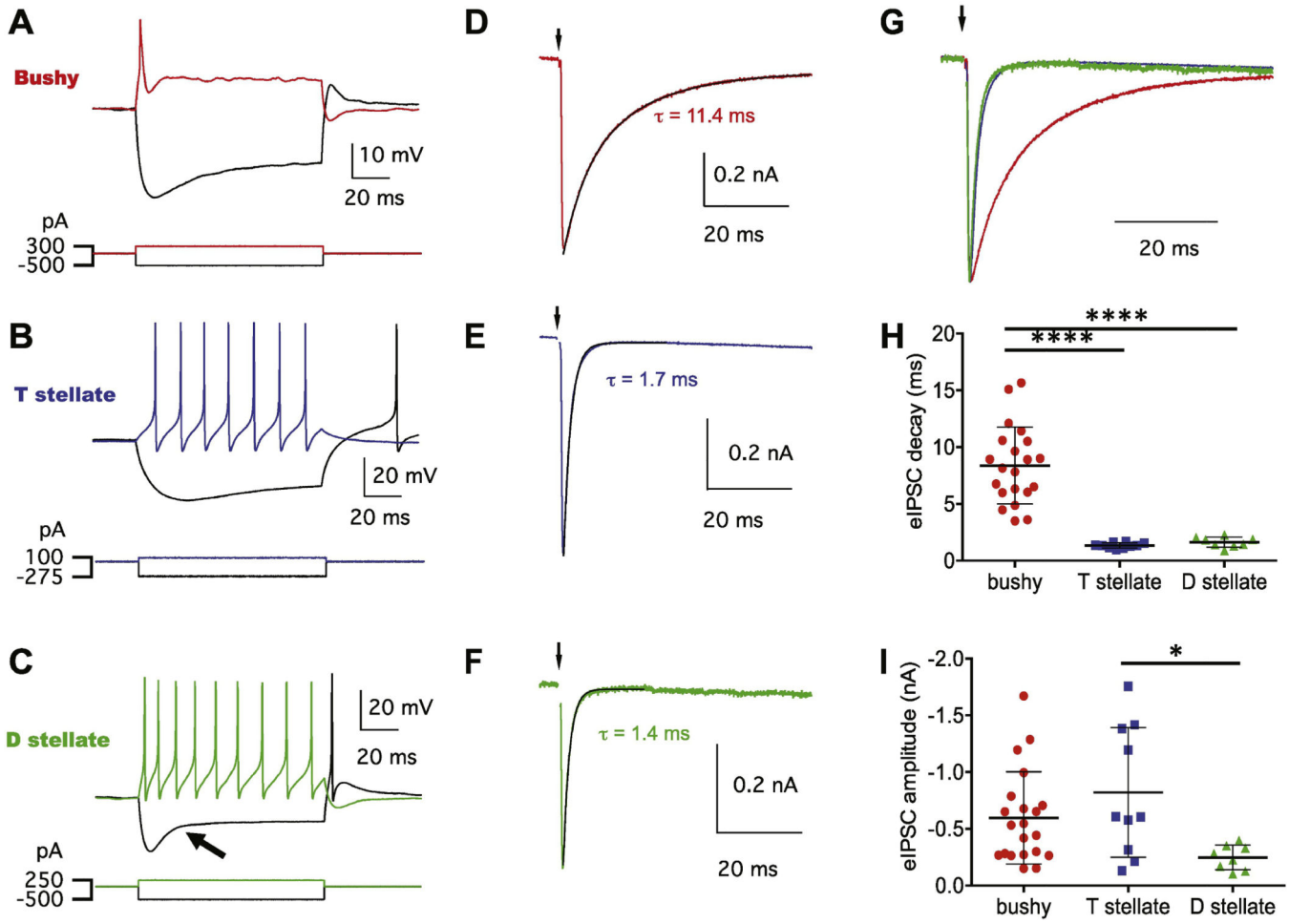

Figure 1.

AVCN principal neurons show cell type-specific elPSC kinetics. (**A-C**) Current pulse injections induced unique response patterns in bushy (**A**), T-stellate (**B**) and D-stellate (**C**) neurons. Note that bushy neurons show transient firing to depolarizing current injections, while both T- and D-stellate neurons show sustained firing pattern. Arrow in (**C**) marks the fast depolarization sag in response to negative current injection in the D-stellate neuron. (**D-F**) elPSCs recorded from the same bushy, T-stellate, and D-stellate neurons in (**A-C**). Traces are average of 20 trials. Black curves show double exponential (**D**) or single exponential curve fittings (**E-F**) to the elPSC decay phase. (**G**) Overlapped elPSCs from (**D-F**) to show kinetic differences; Traces are normalized to the elPSC peak. (**H**) Summary of elPSC decay time constants in three cell types. ****p <0.0001. (I) Summary of elPSC peak amplitude in three cell types. * $p < 0.05$.

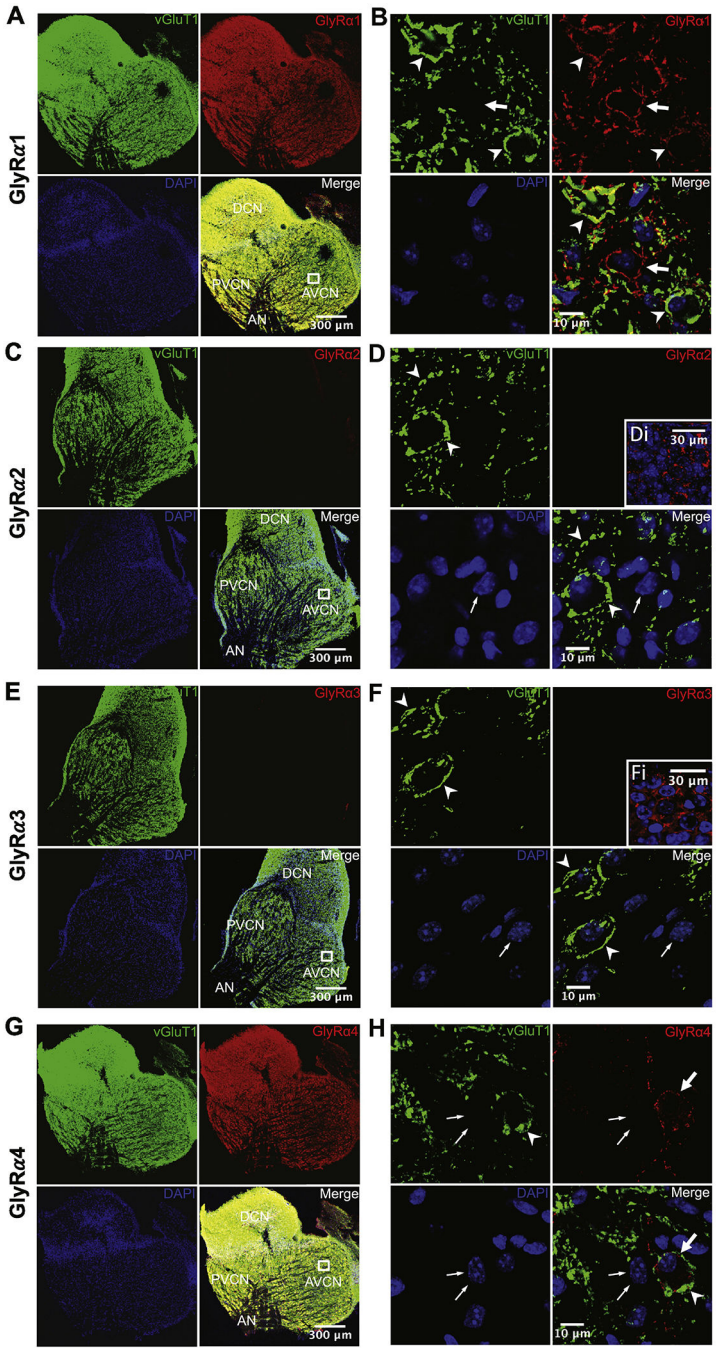

Figure 2.

Cochlear nucleus neurons express glycine receptor α_1 and α_4, but not α_2 and α_3 subunits. Cryostat-sectioned slices of the cochlear nucleus were triple-stained against vGluTl (green), one of the four GlyRα subunits (red), and DAPI (blue). All panels are single frame images taken under a confocal microscope. (**A**) Cochlear nucleus is stained well by GlyRα_1 antibody. Square in the merged panel marks the region of interest in AVCN that is magnified in (**B**). AN: auditory nerve; AVCN: anterior ventral cochlear nucleus; PVCN: posterior ventral cochlear nucleus; DCN: dorsal cochlear nucleus. (**B**) Magnified view of the marked

region of interest in AVCN from (**A**). Arrowhead: example endbulb of Held terminals marked by vGluT1 staining. Arrow: example neuron that is stained well by GlyRα_1 but not by vGluTl. Lack of any endbulb of Held terminal suggests that this neuron is not a bushy but a stellate neuron. (**C**) Cochlear nucleus is not stained by GlyRα_2 antibody. Labels are the same as in (**A**). (**D**) Magnified view of the marked region of interest in (**C**). Arrowheads: two example endbulb of Held terminals stained with vGluT1. Thin arrow: nucleus of a putative stellate neuron with no endbulb of Held terminal. Note: GlyRα_2 does not label any neurons, regardless of whether they receive endbulb of Held terminals or not. Inset (**Di**) : the same GlyRα2 antibody positively labeled neurons in the putative dorsal tier of thalamus of an E14.5 embryonic brain. (**E**) Cochlear nucleus is not stained by GlyRα_3 antibody. (**F**) Magnified view of the marked region of interest in (**E**). Labels are the same as in (**D**). Inset (**Fi**): the same GlyRα_3 antibody positively labeled neurons in mature hippocampus. (**G**) Cochlear nucleus is stained well by GlyRα_4 antibody. (**H**) Magnified view of the marked region of interest in (**G**). Arrowhead: example of an endbulb of Held terminal labeled by the vGluT1 antibody. Thin arrow: example of a putative stellate neuron without endbulb of Held terminals. Arrow: example GlyRα4 staining of a putative bushy neuron with endbulb of Held terminals. Notice in the merged image that the labeled puncta of vGluT1 (green) and GlyRα_4 (red) are interleaved and form the contour of neuronal membrane.

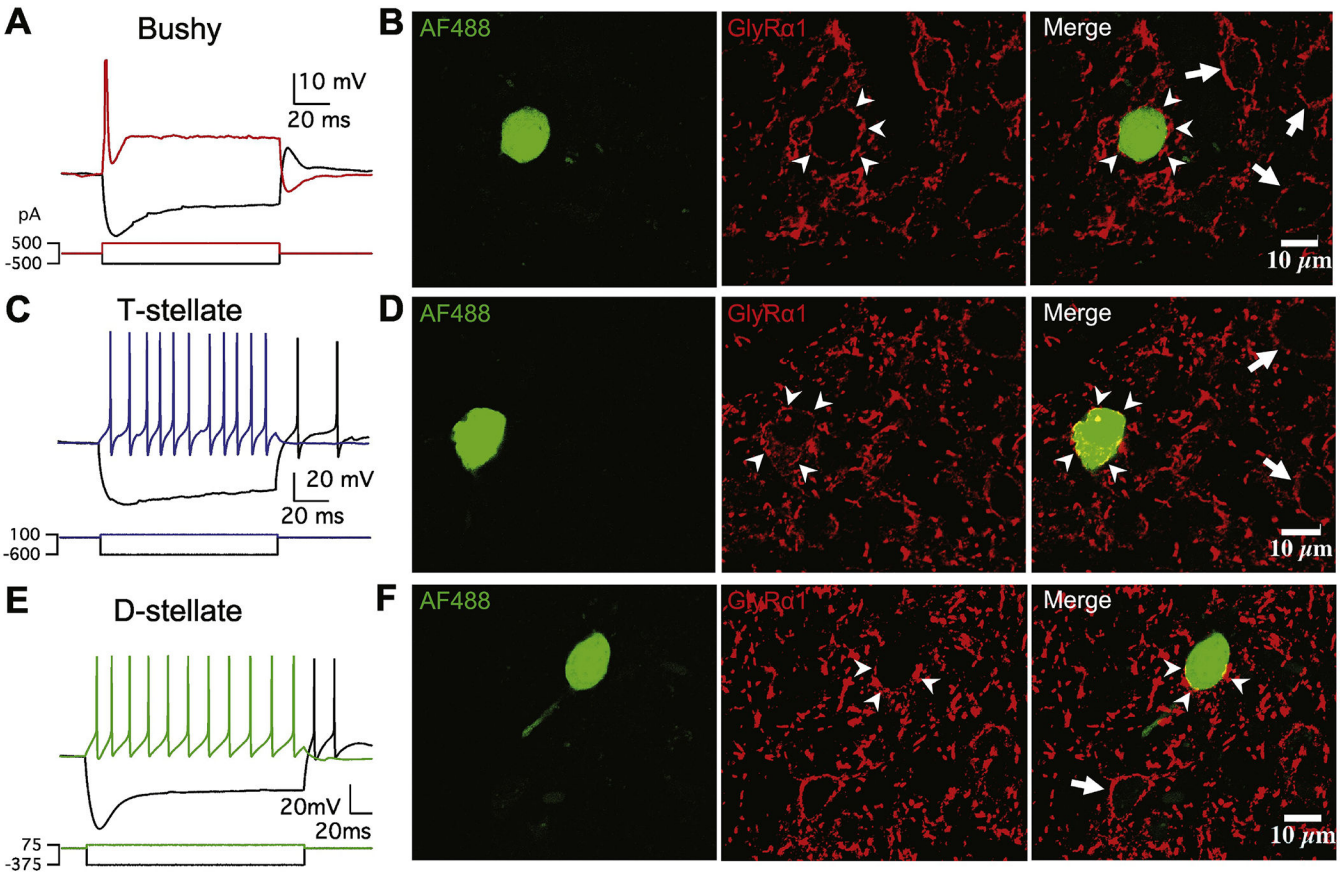

Figure 3.

All three types of principal neurons in AVCN express glycine receptor α_1 subunits. (**A**) Electrophysiological response pattern of an example bushy neuron to current injections. (**B**) The bushy neuron in (**A**) was filled with Alexa Fluor 488 dye (AF488), and the CN slice was fixed and stained with antibody against glycine receptor α_1 subunit (GlyRα_1). Arrowheads: stained GlyRα_1 puncta on the target bushy neuron. Arrows: stained GlyRα_1 puncta on other surrounding neurons. Labels are the same in (**D**) and (**F**). (**C**) Response pattern of an example T-stellate neuron. (**D**) The T-stellate neuron in (**C**) was filled with AF488 and stained by the GlyRα_1 antibody. (**E**) Response pattern of an example D-stellate neuron. (**F**) The D-stellate neuron in (**E**) was filled with AF488 and stained by the GlyRα_1 antibody.

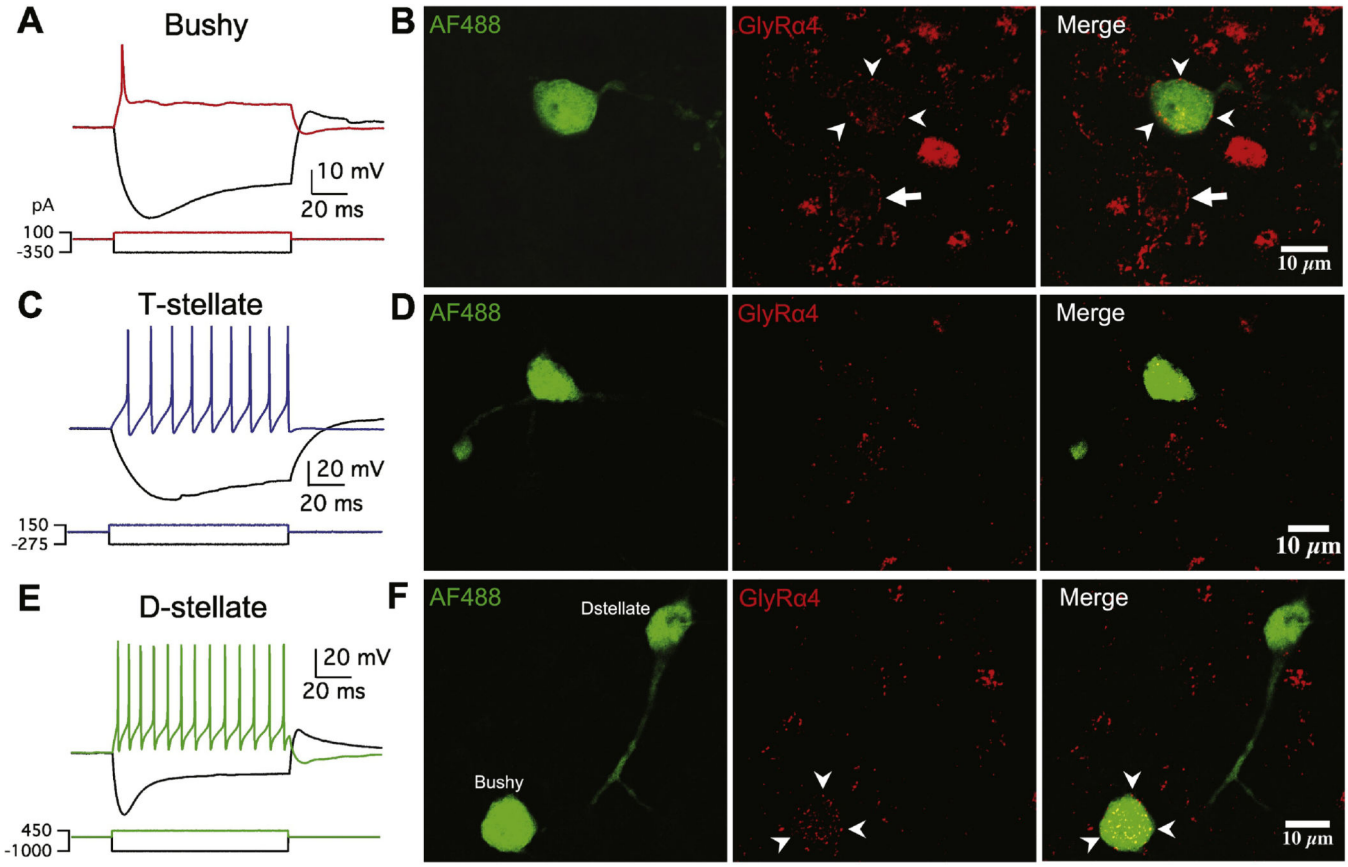

Figure 4.

Only bushy neurons in AVCN express glycine receptor a_4 subunit. (**A**) Electrophysiological response pattern of an example bushy neuron to current injections. (**B**) The bushy neuron in (**A**) was filled with Alexa Fluor 488 dye (AF488), and the CN slice was fixed and stained with an antibody against glycine receptor a_4 subunit (GlyRa_4). Arrowheads: stained GlyRa_4 puncta on the target bushy neuron. Arrow: stained GlyRa_4 puncta on a nearby neuron. (**C**) Response pattern of an example T-stellate neuron. (**D**) The T-stellate neuron in (**C**) was filled with AF488 but was not stained by the GlyRa_4 antibody. (**E**) Response pattern of an example D-stellate neuron. (**F**) The D-stellate neuron in (**E**) was filled with AF488 and was not stained by the GlyRa_4 antibody. Another filled bushy neuron on the same slice was stained by the GlyRa_4 antibody as marked by arrowheads.

Table 1.

Electrophysiological properties of AVCN neurons.

	Bushy (n=21)	T-stellate (n=10)	D-stellate (n=8)	one-way ANOVA/Kruskal-Wallis
Resting membrane potential (mV)	−63.8 ± 1.9	−65.9 ± 3.0	−64.9 ± 1.6	p = 0.0712
Input resistance (MΩ)	53 ± 17	125 ± 77	75 ± 26	p = 0.001**
Membrane time constant (ms)	2.0 ± 0.6	6.6 ± 4.5	2.9 ± 0.9	p = 0.0002***
Threshold current (pA)	290 ± 137	100 ± 123	125 ± 60	p = 0.0002***
Sag time constant (ms)	28 ± 12	52 ± 35	18 ± 8	p = 0.0036**
b/a ratio	0.61 ± 0.12	0.63 ± 0.11	0.49 ± 0.10	p = 0.0434*
eIPSC amplitude (pA)	−596 ± 406	−820 ± 572	−248 ± 109	p = 0.0232*
eIPSC decay time constant (ms)	8.4 ± 3.4	1.3 ± 0.2	1.6 ± 0.4	p < 0.0001****